A Computational Study of Unsteady Ship Airwake

Susan A. Polsky† and Christopher W. S. Bruner*†
Naval Air Warfare Center/Aircraft Division
Bld. 2187, Suite 1320B
Patuxent River, MD, 20670, USA

INTRODUCTION

The superstructure, deck, and other features of large ships produce large separated regions in the airflow over the ship and a variety of vortex flows generated mainly by edges in the geometry. These features are of importance for aircraft operations on and around these ships. The ability to predict the airwake over a ship can aid in the development of aircraft operating envelopes and can be used to "diagnose" airwake structures that result in problematic or unusable landing spots. In addition, the ability to predict airwake could be used as a design tool to address air operations early in a ship design.

To date, wind tunnels have been used almost exclusively to predict ship airwake. The drawback of this approach is twofold. The first issue involves the size of real ships in comparison with the available size of wind tunnels. Because the ships in question are so large, the scale factors required to build reasonably-sized wind tunnel models are generally in the $1/100^{th}$ range. Because of this, the conditions required in a wind tunnel to match full scale Reynolds numbers (Re) are unattainable. Also, unsteady flow phenomena, which are of moderate frequency at full scale, are much higher frequency at wind tunnel scales. These unsteady features are often those of most concern to the pilot. The large scale factors involved introduce Reynolds number and frequency scaling issues when attempting to scale to full-scale values. It can be argued that these flows are largely Reynolds number independent; however, this has not been shown conclusively, and the question of scale is never far from the forefront. Computational fluid dynamics (CFD) has been used in this work as an alternative approach to predicting ship airwake. CFD can be used to compute full-scale solutions and to obtain detailed off-body and time-accurate data.

COMPUTATIONAL METHOD

The CFD solver COBALT (Ref. 1) was used for this study. COBALT is an unstructured-grid, Navier-Stokes solver that is optimized to run in a parallel environment. The code was run in laminar mode. In other words, no traditional Reynolds-average Navier-Stokes (RANS) turbulence model was applied; however, unresolved scales of turbulence were modeled using Monotone Integrated Large Eddy Simulation (MILES) (Ref. 2). MILES turbulence modeling is a form of Large Eddy Simulation (LES) that is inherent in time-accurate, flux-limiting schemes such as the one used in COBALT. The code was run with second-order accuracy in both time and space. The time step used (generally 0.01 seconds) was chosen to resolve frequencies up to 40 Hz based on the Nyquist criterion (Ref 3). Also, although the numerical scheme was unconditionally stable, the size of the time step was limited by time accuracy requirements.

---

† Aerospace Engineer, PolskySA@navair.navy.mil.
* Presently Senior Research Scientist with Combustion Research and Flow Technology, Natl. Ctr. for Phys. Acoustics, University, MS.

Paper presented at the RTO AVT Symposium on "Advanced Flow Management: Part A – Vortex Flows and High Angle of Attack for Military Vehicles", held in Loen, Norway, 7-11 May 2001, and published in RTO-MP-069(I).

Report Documentation Page

Form Approved
OMB No. 0704-0188

1. REPORT DATE	2. REPORT TYPE	3. DATES COVERED
00 MAR 2003	**N/A**	**-**

4. TITLE AND SUBTITLE	5a. CONTRACT NUMBER
A Computational Study of Unsteady Ship Airwake	5b. GRANT NUMBER
	5c. PROGRAM ELEMENT NUMBER
6. AUTHOR(S)	5d. PROJECT NUMBER
	5e. TASK NUMBER
	5f. WORK UNIT NUMBER
7. PERFORMING ORGANIZATION NAME(S) AND ADDRESS(ES) **NATO Research and Technology Organisation BP 25, 7 Rue Ancelle, F-92201 Neuilly-Sue-Seine Cedex, France**	8. PERFORMING ORGANIZATION REPORT NUMBER
9. SPONSORING/MONITORING AGENCY NAME(S) AND ADDRESS(ES)	10. SPONSOR/MONITOR'S ACRONYM(S)
	11. SPONSOR/MONITOR'S REPORT NUMBER(S)

12. DISTRIBUTION/AVAILABILITY STATEMENT
Approved for public release, distribution unlimited

13. SUPPLEMENTARY NOTES
Also see: ADM001490, Presented at RTO Applied Vehicle Technology Panel (AVT) Symposium held inLeon, Norway on 7-11 May 2001, The original document contains color images.

14. ABSTRACT

15. SUBJECT TERMS

16. SECURITY CLASSIFICATION OF:			17. LIMITATION OF ABSTRACT	18. NUMBER OF PAGES	19a. NAME OF RESPONSIBLE PERSON
a. REPORT	b. ABSTRACT	c. THIS PAGE			
unclassified	**unclassified**	**unclassified**	**UU**	**12**	

Standard Form 298 (Rev. 8-98)
Prescribed by ANSI Std Z39-18

COBALT, which is a density-based code, does not have a preconditioner to compensate for the incompressible flow regime studied here. Mach number scaling was used to avoid potential problems associated with applying a density-based CFD code to a flow that is essentially incompressible. The underlying assumption to this approach is that incompressible flows are Mach number independent up to a Mach number of approximately 0.2 to 0.3. This is a fairly common technique to use when a preconditioner is not available. For this study, cases were computed to simulate both full scale and wind tunnel conditions. For the full-scale cases, the Mach number was scaled by a factor of four while keeping the Reynolds number (Re) constant. The highest resulting freestream Mach number used was 0.1814 and the highest Mach number anywhere in the flow was less than 0.3. Mach number scaling was not used for the cases simulating wind tunnel conditions since the Mach number of that flow was already relatively high (0.156).

Unstructured, hybrid grids on the order of 4 million cells were used. The hybrid grids consist of tetrahedra in the inviscid regions and prisms in the viscous layers. The solutions were started impulsively, i.e. with freestream conditions everywhere. They were then run in a time-accurate mode for at least 40 seconds of real time to allow the flow to develop.

The geometry for the ship, an LHA-class Navy ship that is approximately 820ft in length, is shown in Fig. 1. A photo of the actual ship is shown in Fig 1a and the CFD model, along with a top view showing the wind direction convention, is shown in Fig. 1b. There is considerable detail represented in the CFD model including the major features of the island, the deck and hull shape, the deck edge elevator, and the deck crane. The main features that have been neglected are the “yellow gear” (equipment used in daily operations) and the antenna arrays on the island. The yellow gear were neglected mainly because the various pieces of equipment are relatively small (compared to the size of the ship) and because they are not in fixed positions. The antenna arrays were neglected mainly due to the difficulty of modeling the complex antenna geometry.

The full-scale LHA solutions were run on an IBM P3 using 64 processors. Each solution required at least 4000 iterations and approximately 128 hours of wall-clock time which was equivalent to approximately 8,000 hours of cpu time per solution. Of the 4000 iterations, 1000 iterations were considered to be initialization and the remaining 3000 iterations, equivalent to 30 seconds, were considered to be the fully initialized, time-accurate solution set. The time steps were set to 0.01 seconds and 0.0025 seconds for the initialization stage and data acquisition stage, respectively.

VALIDATION

Validation of CFD simulations when a code is applied to a new class of problems is always an important step. Both wind tunnel data and full-scale data were used for the validation study. Wind tunnel data will be examined first.

Validation with Wind Tunnel Data

Wind tunnel data was acquired at the NASA Ames Fluid Mechanics Lab (Ref. 4). The model geometry and the plane in which data were taken are shown in Fig. 2. The test article was a simplified version of an LHA at $1/120^{th}$ scale. The test article caused a significant amount of blockage in the tunnel; therefore, the CFD simulation included the tunnel walls.

The data were non-dimensionalized by the tunnel speed, 170 ft/s. A seven-hole probe was used to collect three-component velocity data. It should be noted that a seven-hole probe records time-averaged values of velocity. Therefore, unsteady aspects of the flow were not detected. As is discussed below, the unsteady nature of the flow and the type of data acquisition impact how the computational simulations must be conducted and post-processed, respectively.

The CFD solutions were run with second order time accuracy in order to resolve the unsteady nature of the flowfield. The solution was run for 2000 steps to initialize the flow and then time-accurate velocity data were

collected over 0.356 seconds. The 0.356-second time period consisted of 17,800 time steps of 2×10^{-5} seconds each. The 17,800 samples of each velocity component were then averaged over time in order to compare directly with the seven-hole probe data.

Comparisons of the wind tunnel and CFD data for increasing heights off the deck are shown in Figs. 3a-3b. The data compare very well, and the major flow features such as the two deck-edge vortices are clearly indicated in the CFD data as a rapid dip and jump near y = +/-6 inches. Note that the data are not symmetric about y=0. This is due to the upstream influence of the island.

In these figures, x runs longitudinally down the ship, y runs across the ship from port to starboard, and z runs from the deck surface up. A y-value of 0 indicates the centerline of the ship. The u, v, and w components of velocity correspond to x, y, and z coordinate directions, respectively. The width of the ship lies from approximately -6 inches to + 6 inches in y.

Time Accurate vs. Steady State CFD

It has been argued that even if a flow contains some unsteady features, a converged, steady-state CFD solution should result in a time averaged solution of the actual flowfield; however, that is not the case for this flow. The time-averaged u, v, and w velocity components for a deck height of 0.7315 inches (7.315 feet full scale) are plotted in Figs. 4a-c. Also plotted in these figures are the results from a converged, steady-state solution. As these figures demonstrate, the steady-state solution does not give the same results as the time-averaged solutions. More importantly, the steady-state results do not compare nearly as well to experiment as the time-averaged results. This is especially true of the v-velocity components near the ship centerline where the steady-state values are in significant error. The differences are most likely attributable to the fact that steady CFD solutions obtained using local time-stepping (that is, integration with constant CFL number) are physically correct only when fully converged. An unsteady flow never achieves convergence (in the sense of a small residual). Hence, while local time-stepping is a powerful technique for steady problems, application of local time-stepping is inappropriate for problems with significant unsteadiness.

Validation with Full-scale Data

Full-scale data was gathered over two separate ship tests. The data was taken using four ultrasonic anemometers positioned at the top of 20ft poles (Fig. 5). The four poles were positioned at various locations around the deck to map out mainly the bow, spot 2 and spot 7 (Fig. 1b) for several wind-over-deck (WOD) conditions. For each location, two minutes of data was recorded at a frequency of 20Hz. A large amount of data was gathered; however, only a preliminary analysis at one anemometer location will be shown in this work.

Data traces for three velocity components are shown in Fig 6. These traces were recorded by a single anemometer near Spot 7 in a relative wind of 10° and 30kts. The velocities computed by the CFD (also sampled at 20Hz) are also shown. Note that the traces are not time correlated (i.e. they both arbitrarily start at time=0 seconds). Note also that the full-scale data is non-stationary due to changes in the ambient wind over the recording period. The experimental and CFD data were both processed to produce power spectral density (PSD) plots. Neither of the data traces were preprocessed for trend removal, etc. The PSD plots are shown in Fig 7. Matlab was used to create the PSDs with an NFFT=512 which results in approximately five averages. Two CFD solutions are shown. The first, labeled “CFD”, uses MILES turbulence modeling as discussed above. The second curve, labeled “CFD w/SST Turbulence” was run with a Menter’s SST (shear stress transport) boundary layer turbulence model (Ref. 5). Looking at the experimental data and the first CFD curve, one can see that the CFD predicts similar frequency content at approximately 0.1Hz, 0.4Hz and perhaps 0.8Hz. The amplitudes also agree fairly well. It is interesting to note that the CFD run with the SST model compares very well with the experimental data at the lowest frequency (0.1Hz). Unfortunately, the SST turbulence model damps out any higher frequency data. This over damping was anticipated because past research has

shown that flux-splitting numerical schemes have some level of boundary layer turbulence modeling inherent in the scheme (see discussion of MILES turbulence modeling in the Numerical Methods section). Therefore applying an additional turbulence model tends to add too much dissipation to the calculation. This calculation seems to bare that out. Overall, the agreement between the CFD (MILES calculation) and the full-scale data is very encouraging. Further analysis of the full-scale data will be presented in a future work.

Reynolds Number & WOD Speed Independence

Because each time-accurate solution requires over 5 days of wall clock time to obtain 30 seconds of results, it would be nearly impossible to obtain results for every wind speed and angle that the ship would experience. As is discussed below, the flow changes dramatically as the wind angle changes, so there is little choice but to run a separate case for each wind angle of interest. However, it appears that the flowfield's structure does not change much when varying the wind speed. In other words, an LHA flowfield at 330° and 15kts is essentially the same as the flowfield at 330° and 30kts except that it is moving at half the speed. As was reported in Ref. 6, two solutions were computed with 15- and 30-knot wind speeds and a constant wind angle of 330°. The solution from the 30-knot case was then scaled down to 15 knots by dividing the velocity components by a factor of two. Comparisons of velocity magnitudes between the two cases were made along the ship centerline, along a typical approach path, and across several landing spots. For all the locations examined, the profiles compared very well. As an example, plots of surface pressure coefficients for a WOD of 15 knot and 30 knot at 330° are shown in Fig. 8. Note that the plots shown in Fig. 8 (reproduced from Ref. 6) were created at a solution time equivalent to 4 seconds after the impulsive start.

Because the WOD=0° case has substantially different aerodynamic characteristics than the oblique wind angles (due to the reattachment of the bow separation) velocity (i.e. Re) scaling for this case also be examined. Changing the Re could potentially change the reattachment which in turn could alter the downstream flow significantly. For the oblique wind cases, the flow over the ship is massively separated, and there is no significant reattachment near or on the ship that could affect important near field wake characteristics. Computations were made for 15-knot and 30-knot winds straight down the bow. Surface pressure plots for each case at time=50sec are shown in Fig. 9. The separated region at the bow is indicated by the area of low pressure (blue in color or dark gray in grayscale figures). A reattachment line is indicated where the pressure suddenly increases. As is shown in the figure, the reattachment regions for the 15- and 30-knot cases occur in essentially the same place.

As was concluded in Ref. 6, based on the above Re independence, only one solution need be run for each wind angle of interest. In other words, a 30kt solution can be scaled directly to any wind speed of interest within limits. If the speed is scaled too high, compressibility effects will corrupt the solution. Similarly, as the speed approaches zero, the flow will look very different from that at 15 knots. Therefore, a minimum of two speeds must always be computed (the maximum and minimum speeds of interest) before scaling can be performed with confidence.

As was discussed above, the velocity magnitude along the ship's centerline for the WOD=15- and 30-knot, 330° cases at time=4sec compared very well. This is also true for the WOD = 0° case as shown in Fig 10. However, it has since been found that 4 seconds is much too early to make this comparison. Indeed, as the flow continues to develop, the velocity traces begin to diverge from one another, Fig 11. Despite this fact, the overall flow field structures remain very similar. Iso-surfaces of vorticity are shown in Fig 12 for the same equivalent time (50seconds) for both the 30kt and 15kt cases. The comparison seems to indicate that there is some frequency dependence being induced by the Re difference that causes the two flow fields to become unsynchronized. In other words, the shedding frequencies do not exactly scale linearly with Re. While numerical aspects (how the code was run) may also contribute to differences in the two calculations, as many variables as possible were held constant including time-step, flow speed, CFL number, damping and grid. The change in Re was achieved by scaling the pressure; otherwise the two calculations were run exactly the same.

Although the 15- and 30- knot flows do not remain exactly alike as time progresses, the overall structure is indeed very similar. Therefore, at least for calculations destined for manned flight simulation, it is still concluded that once a flow field at a given wind speed and (fixed) angle has been calculated, the velocity field can then be linearly scaled to other wind speeds of interest.

It is very important to note that the Re variation being discussed here is only a factor of 2 (from 15 to 30 knots) – not a factor 50+ that is required to scale wind tunnel experiments. Therefore, the Re independence seen here may not hold for wind tunnel applications. This issue will be explored in a future work.

Variations in Wind Angle

The changes in the flow features as the wind-over-deck angle is changed are demonstrated in Fig. 15. Here, seven WOD conditions are shown from a top view of the ship. It is easy to see how dramatically the flow field changes with changing wind direction. In this study, a total of 70 seconds of flow time was computed for each case. After examining several cases, it was determined that after 40 seconds had elapsed the flow was well established and most transients due to the impulsive start had flushed out of the domain. The remaining 30+ seconds of data were used for analysis.

Two cases are analyzed in detail. The first case presented is for a WOD of 30 knots and 0°. Surface pressure contours at an instant in time are shown at the top of Fig. 9. Much can be learned about the flow based on this figure such as the existence of a large separation at the bow indicated by the distinct low-pressure region (shown in blue). However, the truly complex nature of the flowfield is not revealed until the off-body flow is examined. Iso-surfaces of vorticity are shown in Fig. 13. The separation off the bow is much clearer in this figure. In addition, deck-edge vortices are easily seen. Significantly, the voritcity iso-surfaces reveal “burbles” in the flow field between the bow-separation and the island. Also, the highly complex nature of the flow around and behind the island is indicated. When the solution was animated, it was found that the “burbles” are shed periodically from the bow separation at a frequency of approximately 0.2-0.3Hz (i.e. shedding every 3-5 seconds). It also appears that the shedding from the bow separation excites the deck edge vortices causing them to “bulge”. The bulge in the vortex persists downstream until geometric features or other flow features disturb it. The burbles impinge on the island and interact with the island separation. All this feeds back into the area behind the island where the flow is highly separated and very complicated. In general, the flow behind the island is very unsteady and, thus far, features in this region appear to be relatively random.

The second case is again for a wind speed of 30 knots; however, the wind direction is now 30° (Fig. 14). The major flow features have changed dramatically from the 0° case. First, the separation off the bow is almost nonexistent in the 30° case. Since the bow separation was the driver to create the periodic shedding of the “burbles”, these features do not appear in this flow. In addition, there is a significant separation off the starboard deck edge and considerably more of the leeward island flow is separated. The starboard deck-edge vortex is blown across the deck, and the port-side deck-edge vortex is detached from the deck and blown out over the ocean. The flow behind the island is more dramatically separated, and there does seem to be some periodic shedding off the island itself; however, this has not yet been confirmed by animating the solution.

Integration into Manned Simulation Environment

All seven wind conditions have been integrated (Ref. 7) into a UH-60A helicopter simulation model at the NASA Ames Vertical Motion Simulator (VMS) through the Joint Ship Helicopter Integration Process (JSHIP) program which sponsored much of this work. The VMS was provided 3-component velocity data on a subset of the CFD volume grid (Fig. 16). The VMS grid size was kept as small as possible (56,661 points) and encompassed only the port side of the ship 1000 ft out from the port deck edge. The size and shape of the grid was chosen to cover the space used for approaches and departures for the UH-60A. The number of points in the grid was kept small so that the data could be handled in a real time environment. Preliminary test flights

were completed in the simulator using the airwake for 0°, 30°, and 330°. Pilot feedback was very positive concerning the realism of the airwake effects.

CONCLUSIONS

Time-accurate data for an LHA ship airwake were computed using CFD. The resulting velocity data were compared against both wind tunnel and full-scale data. Time-accurate CFD data averaged over time compared very well to the 7-hole probe velocity data gathered in the wind tunnel. It was shown, however, that steady-state CFD calculations did not compare well and were inappropriate to use for highly unsteady flow fields such as ship airwake. Preliminary investigations showed that full-scale CFD calculations were able to predict the dominant frequencies in the flow field. When a standard two-equation turbulence model was used, however, the higher frequencies were completely damped out.

It was demonstrated that for the Reynolds numbers of interest (3.22×10^5/ft and 1.61×10^5/ft for 30kts and 15kts, respectively) the flow is largely Re independent. It was concluded, therefore, that although a new CFD calculation must be made for each new wind angle, only one solution need be made in the 15-30kts speed range which can then be scaled linearly to other speeds of interest within that range. It was shown that the character of the overall flow field changed dramatically as the wind angle was changed. For winds down the bow, periodic shedding was observed from the bow separation. This shedding was not evident for beam wind angles (such as 90°) where the flow was dominated by massive separation from the island structure.

CFD has been shown to be a promising tool for ship airwake prediction and analysis. Future work will more thoroughly examine the available full-scale data, will explored numerical issues such as time accuracy and grid resolution, and will examine scaling issues associated with wind tunnel data.

REFERENCES

[1] W. Strang, R. Tomaro, and M. Grismer, "The Defining Methods of $Cobalt_{60}$: A Parallel, Implicit, Unstructured Euler/Navier-Stokes Flow Solver", AIAA Paper 99-0786, Jan. 1999

[2] J. Boris, F. Grinstein, E. Oran, R. Kolbe, "New Insights into Large Eddy Simulation", Fluid Dynamics Research 10 (1992) 199-228.

[3] Bendat and Peirsol, "Random Data Analysis and Measurement Procedures", Wiley-Interscience Pub., 1986.

[4] Private communications with Kurt Long, NAWCAD, Patuxent River, MD and NASA Ames Fluid Mechanics Lab, Moffet Field, Ca., 1999.

[5] Menter, F. R., "Zonal Two Equation k-ω Turbulence Models for Aerodynamic Flows", AIAA 93-2906, July 1993.

[6] Polsky, S. A., Bruner, C. W., "Time-Accurate Computational Simulations of an LHA Ship Airwake", AIAA-2000-4126, August, 2000.

[7] Bunnel, John, "An Integrated Time-Varying Airwake in a UH-60 Black Hawk Shipboard Landing Simulation", AIAA-2001-4065, August, 2001.

Fig 1a. LHA-2, the USS *Saipan*.

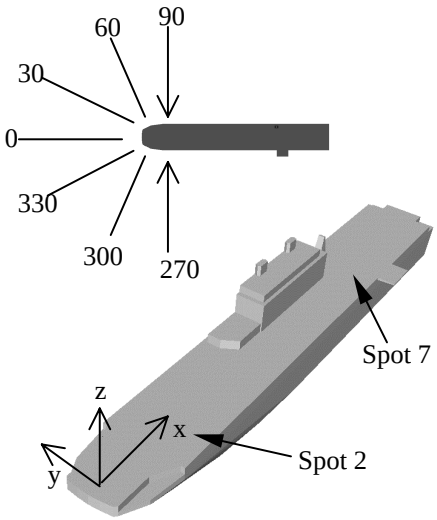

Fig 1b. CFD Model of an LHA and WOD Azimuths (top)

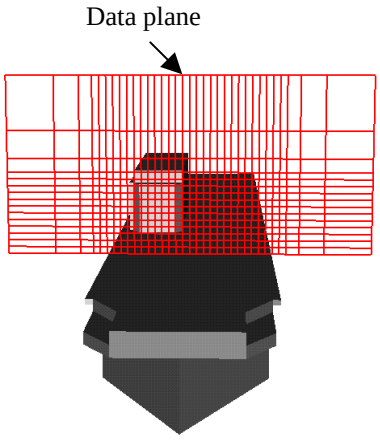

Fig 2. Wind Tunnel Model of LHA

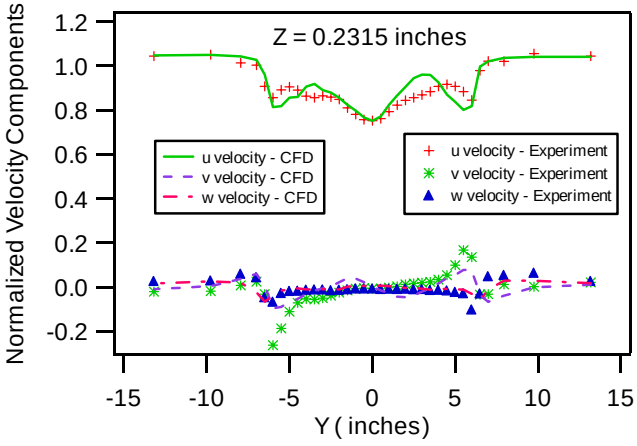

Fig 3a. Comparison of Wind Tunnel and CFD for u,v,w velocity components, Z=0.2315in.

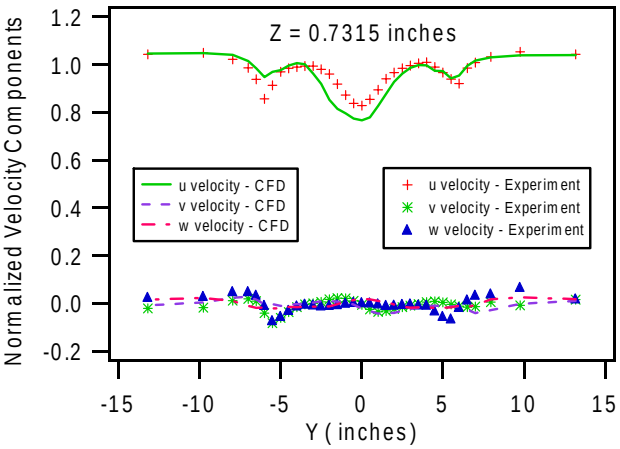

Fig 3b. Comparison of Wind Tunnel and CFD for u,v,w velocity components, Z=0.7315in.

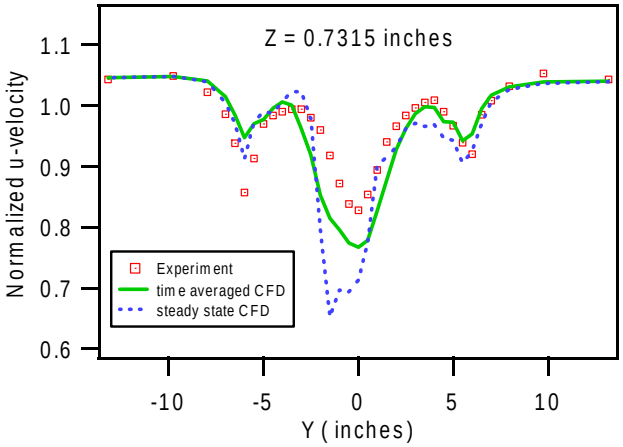

Fig 4a. Comparison of u-velocity for Wind Tunnel and CFD Data, Z=0.7315in.

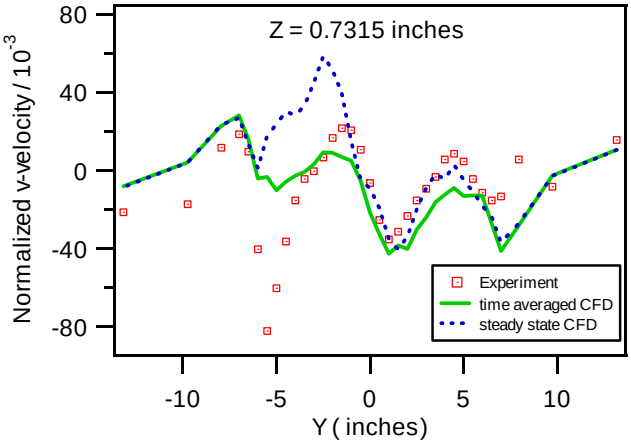

Fig 4b. Comparison of v-velocity for Wind Tunnel and CFD Data, Z=0.7315in.

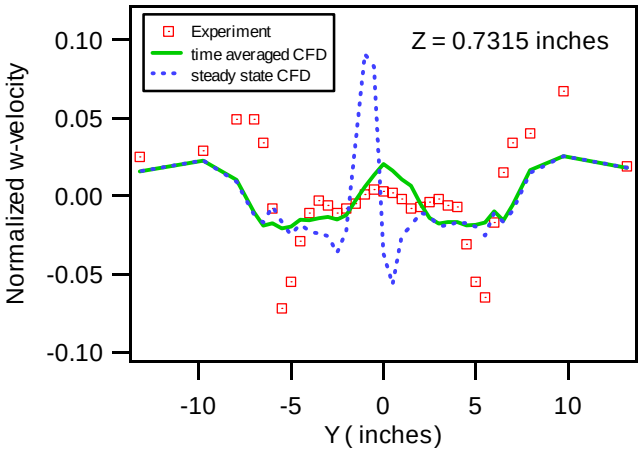

Fig 4c. Comparison of w-velocity for Wind Tunnel and CFD Data, Z=0.7315in.

Fig 5. Four Ultrasonic Anemometers Atop 20ft Poles Used for Full-scale Data Collection

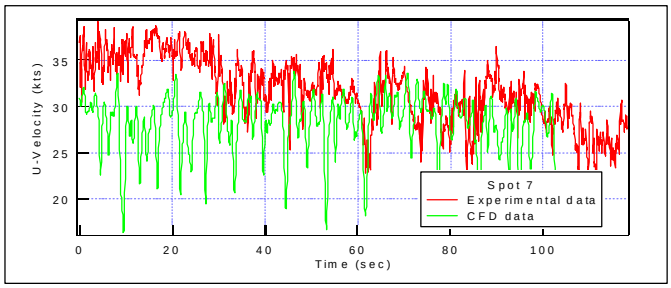

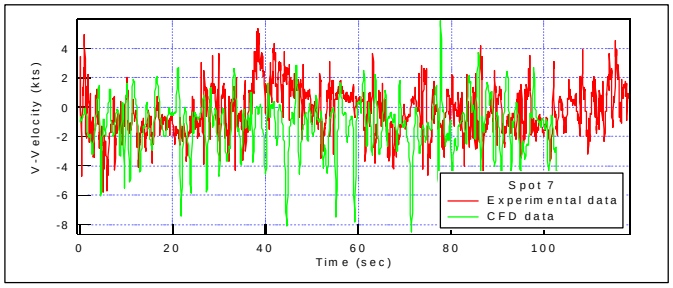

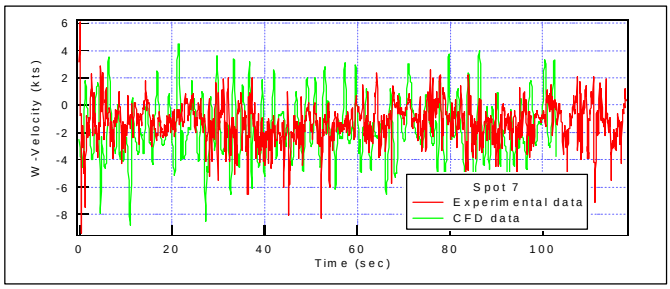

Fig 6. Time Histories of u,v,w velocity components for Experimental and CFD Data.

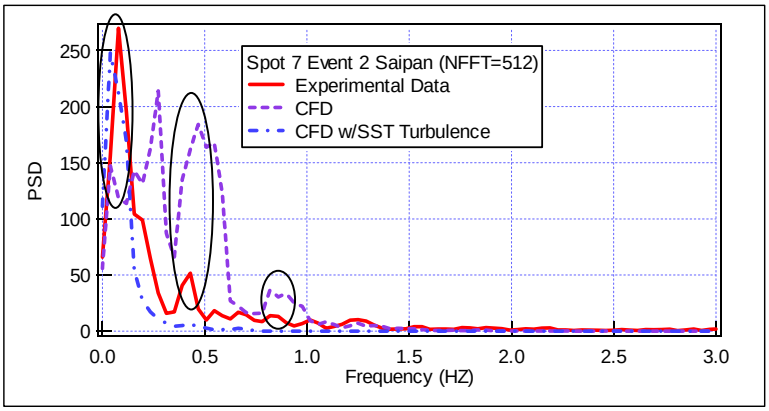

Fig 7. PSD of Experimental and CFD U-Velocity Data 20ft Off the Deck.

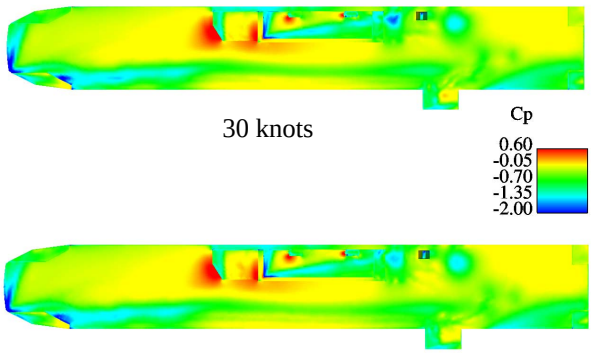

Fig 8. Surface Pressure Coefficient, Cp, for Two Different Reynolds Numbers. WOD=330º

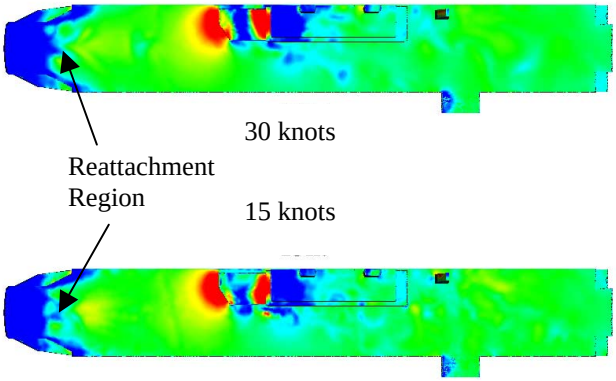

Fig 9. Surface Pressure Coefficient, Cp, for Two Reynolds Numbers. WOD=0º, t=50sec

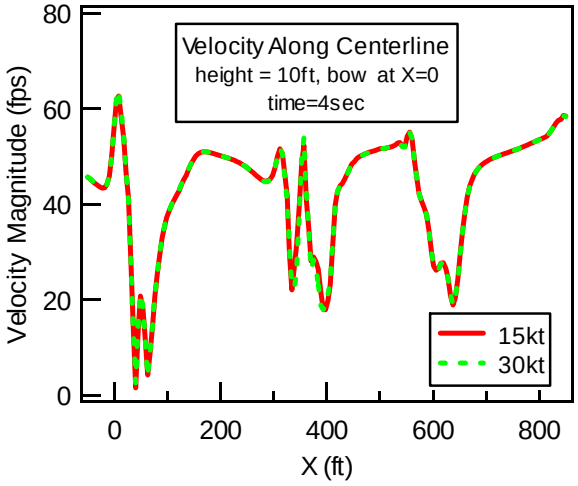

Fig 10. Centerline Velocity Comparison for Two Different Reynolds Numbers, WOD=0º.

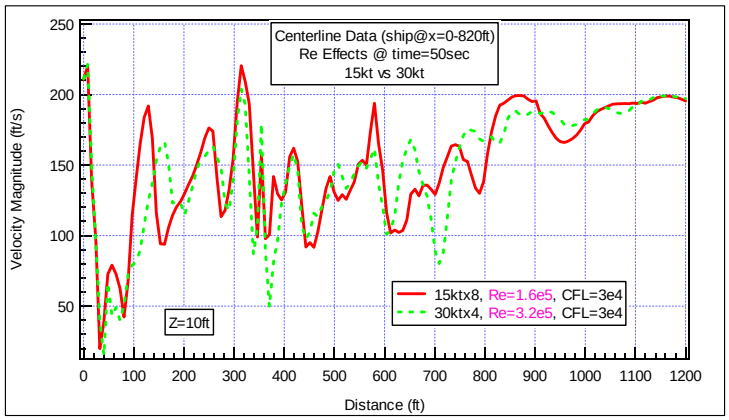

Fig 11. Centerline Data at time=50sec for Two Re Numbers (ship @ distance=0-820ft)

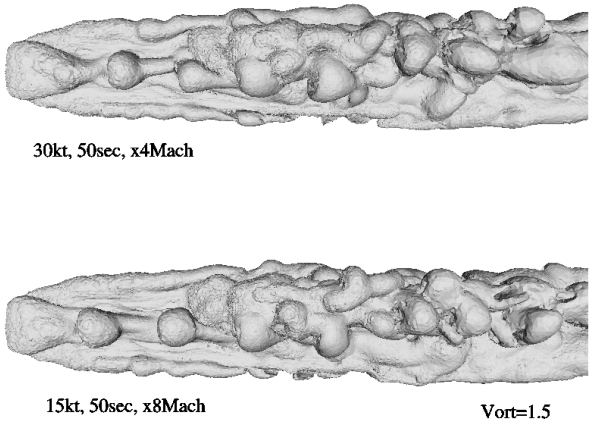

Fig 12. Iso-surfaces of Vorticity Comparing Two Different Re (top view)

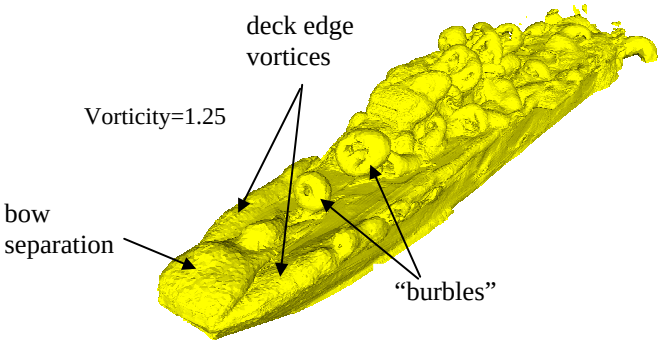

Fig 13. A Snapshot in Time of Vorticity iso-surfaces for WOD=0º, 30kt

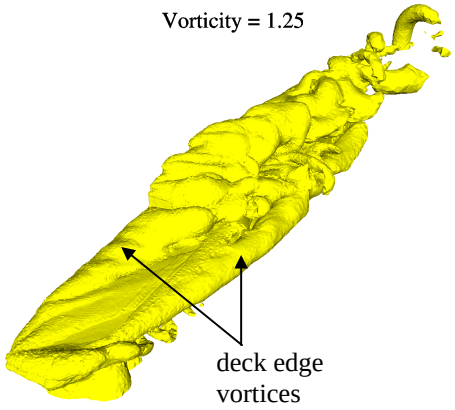

Fig 14. A Snapshot in Time of Vorticity iso-surfaces for WOD=30º, 30kt

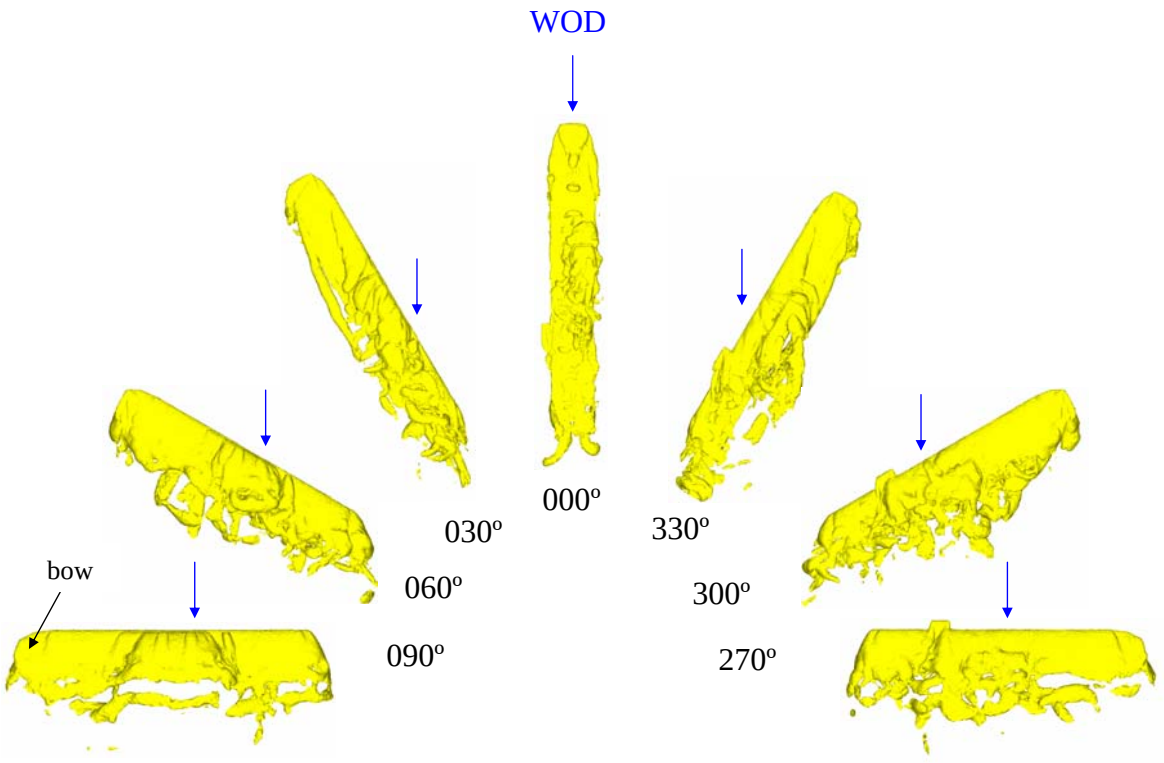

Fig 15. Iso-surfaces of vorticity demonstrate flow variations for seven WOD angles (top view, bow toward outside of figure, wind direction indicated by blue arrow).

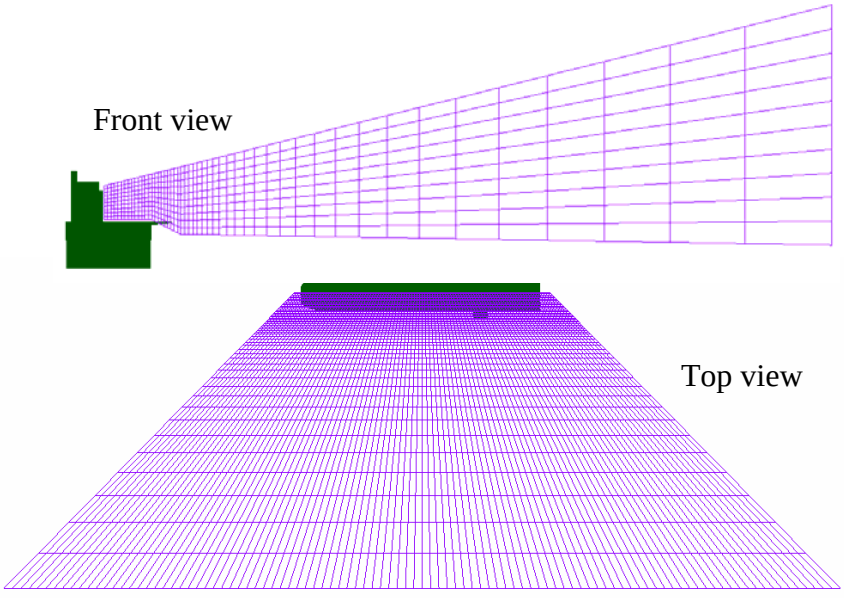

Fig 16. Velocity data from the unstructured computational grid was interpolated onto a Cartesian grid to supply data to the manned flight simulator.

Paper: 25
Author: Ms. Polsky

Question by Dr. Mokry: How did you model the water surface in your computation?

Answer: The water surface was modeled as a flat, inviscid, solid surface.

This page has been deliberately left blank

Page intentionnellement blanche